Expanded View Figures

Figure EV1. TRF2 overexpression in cancer cells induces a strong immunosuppressive microenvironment via the recruitment of MDSCs and regulatory T cells.

A–D Analysis of immune cell infiltration in TRF2-overexpressing or TRF2-knockdown B16F10 melanoma tumors. Box plots of total immune cell infiltration ($CD45^+$ cells), total T cell infiltration ($CD45^+$ $CD3^+$ T cells), and $CD8^+$ or $CD4^+$ T cells among $CD3^+$ cells infiltrating (A). Representative density plot of regulatory T cells ($CD25^+$ $Foxp3^+$ Treg) and activated T cells ($CD25^+$ $Foxp3^-$) (B). Box plots of infiltrating Treg ($CD25^+$ $Foxp3^+$) and activated T cells ($CD25^+$ $Foxp3^-$) (C) or NK cells ($NKp46^+$ $CD3^-$) (D).

E Analysis of MDSC infiltration in TRF2-overexpressing or TRF2-knockdown BJcl2 tumors in Nude mice.

F, G Data used for the correlation analysis presented in Fig 1F–I. Box plots present the percentages of $CD11b^{Hi}$ $GR1^{Hi}$ MDSCs among $CD45^+$ cells infiltrating the Matrigel plug, the mean fluorescence intensity (MFI) of intranuclear pSTAT3 staining in MDSCs, the percentages of intratumoral $CD3^-$ $NKp46^+$ NK cells among $CD45^+$ cells, and $NKp46^+$ IFN-γ^+ NK cells (F). The mRNA expression level (relative quantity) in the Matrigel plugs of arg1, tgfβ, and il-10.

Data information: In (A–D), data are presented as box plots min to max showing all points with median from $n = 5$ or 10 tumor-bearing mice per group (*$P < 0.05$, **$P < 0.01$, and ***$P < 0.001$, Mann–Whitney test). In (E), data are presented as box plots min to max showing all points with median from $n = 8$ tumor-bearing mice per group. In (F–G), data are presented as box plots min to max showing all points with median from $n = 8$ mice per group of Matrigel plug assay (*$P < 0.05$, **$P < 0.01$, and ***$P < 0.001$, Mann–Whitney test).

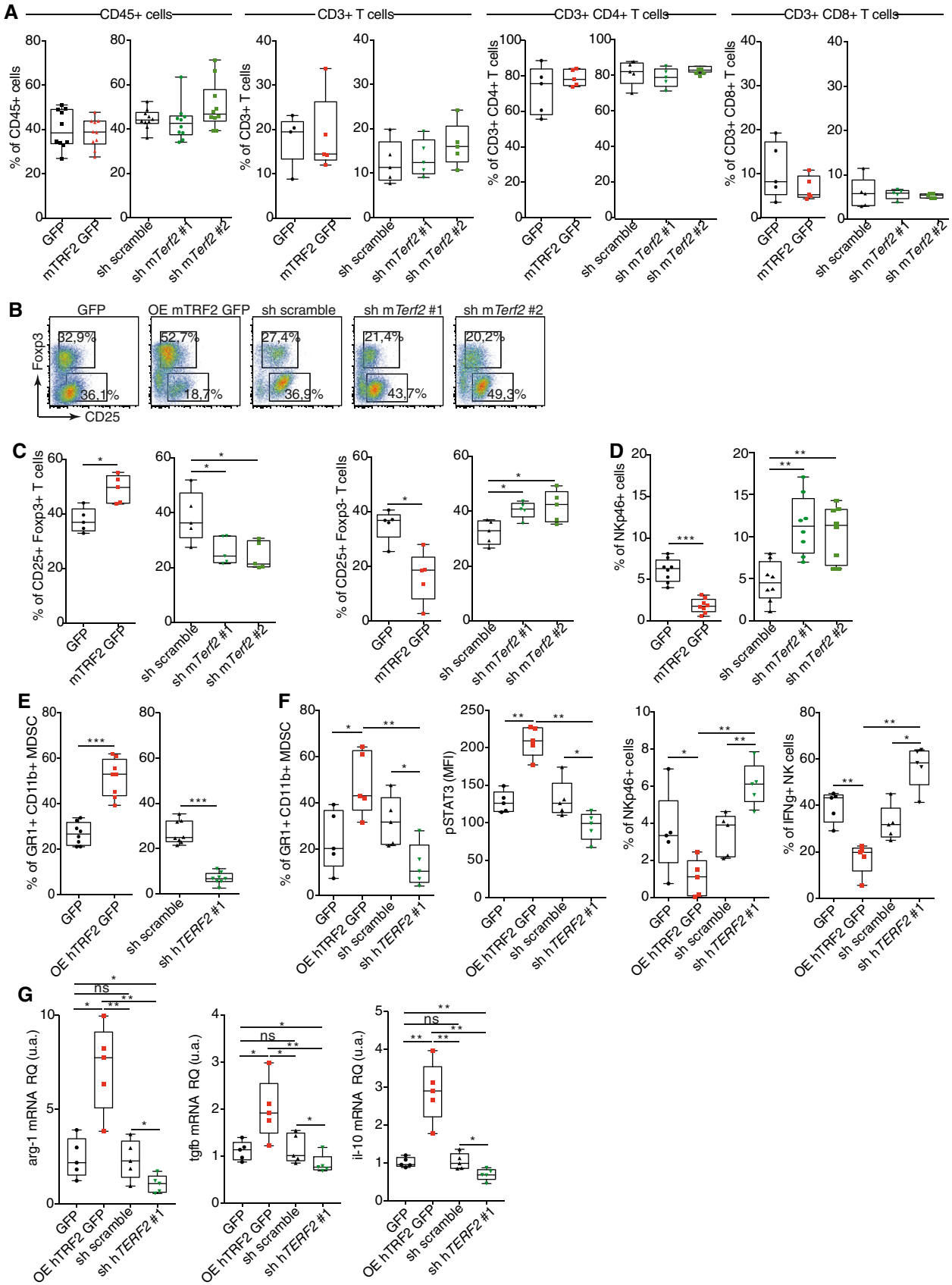

Figure EV1.

Figure EV2. The TRF2-dependent immunosuppression is abolished by MDSC depletion.

A B16F10 tumor volumes before (left panel) and tumor volume and weight after anti-GR1 depletion (right panel).
B B16F10 GFP^+ metastasis infiltrating lung from subcutaneous tumor-bearing mice (from panel A) after anti-GR1 depletion.
C Total immune cell infiltration ($CD45^+$ cells), total T cell infiltration ($CD45^+$ $CD3^+$ T cells), and $CD8^+$ or $CD4^+$ T cells among $CD3^+$ cells in TRF2-overexpressing or TRF2-knockdown B16F10 tumors treated with or without the anti-GR1 antibody (from panel A).
D The mRNA expression level (relative quantity) in the tumors of arg1, tgfβ, and il-10.
E PMN-MDSCs and M-MDSCs distribution among total intratumoral MDSCs in B16F10 TRF2-overexpressing tumors after anti-GR1 depletion.
F Density plot of infiltrating M-MDSCs, PMN-MDSCs, total NK cells, and $CD107a^+$ or $CD69^+$ NK cells in control or anti-GR1-treated Matrigel plugs generated with BJcl2 cells.
G–K Matrigel plug assay using B16F10 cells in anti-GR1 treated animals (G). Total immune cell infiltration ($CD45^+$ cells) (H), total T cell infiltration (H), MDSCs (I), total NK cells (J), and activated NK cells (K).

Data information: All experiments are performed with $n = 8$ mice per group; $^*P < 0.05$, $^{**}P < 0.01$, and $^{***}P < 0.001$; Mann–Whitney test.

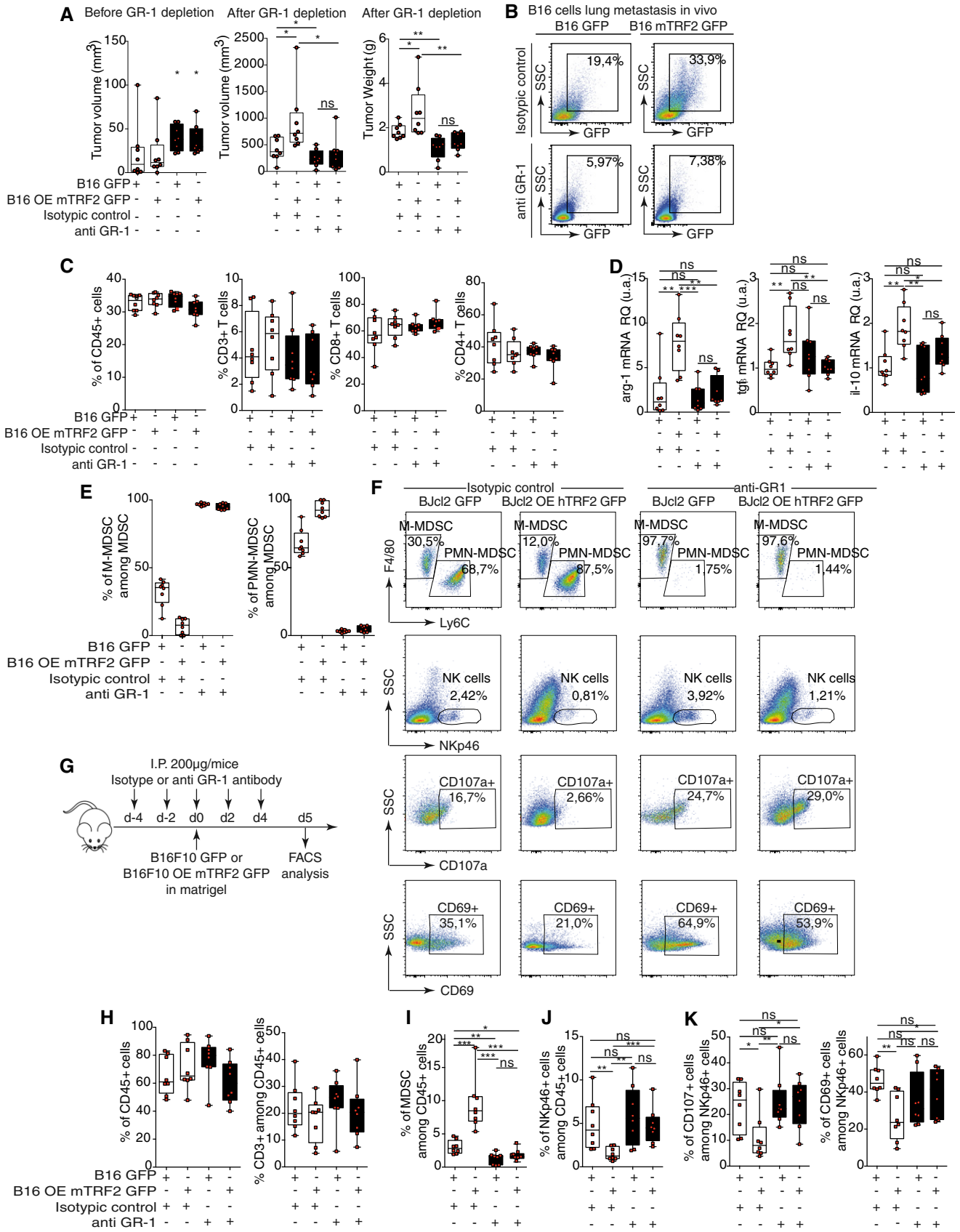

Figure EV2.

Figure EV3. TRF2-mediated regulation of MDSCs via TLR2/MyD88 pathway inhibits NK cell functionality.

A Density plot of CD11b GR1 staining in MSC2 cells.
B MSC2 cells were activated with 1 μM lipopolysaccharide (LPS), and pSTAT3 levels were determined 18 h after stimulation by FACS.
C STAT3 phosphorylation by MSC2 cells after co-culture with BJcl2 (left panel) or B16F10 cells (right panel) overexpressing or knockdown for terf2.
D, E STAT3 phosphorylation by MSC2 cells after co-culture with conditioned media from BJcl2 (left panel) or B16F10 (right panel) overexpressing or knockdown for terf2.
F, G Dose–response analysis of pSTAT3 levels in MSC2 cells after treatment with various doses of the TLR4 antagonist LPS-RS, anti-mouse TLR2 antibody, or anti-MyD88 peptide (F) or with various doses of anti-mouse IL-6 antibody or JAK1/2 inhibitor (G).
H Histograms of the pSTAT3 MFIs depending on the concentration of the molecule.
I MSC2 cell number after 18 h of co-culture with BJcl2 cells ± anti-mouse IL-6 antibody or JAK1/2 inhibitor.
J Representative density plot to assessed purity control for MSC2 sorting from the co-culture or NK cell sorting from splenocytes.
K–M Schematic representation of the MDSC suppression assay (K). TRF2-overexpressing or TRF2-knockdown B16F10 cells were co-cultured with MSC2 cells for 18 h. After FACS sorting, MSC2 cells were co-cultured for 18 h with primed and purified NK cells before a 4 h challenge with YAK-1 E/T ratio of 5:1. NK cell degranulation (L) and IFN-γ production (M) were analyzed by FACS.

Data information: Data are presented by showing all points with mean ± SEM (n = 3 independent experiments; *$P < 0.05$, **$P < 0.01$, and ***$P < 0.001$; Student's t-test).

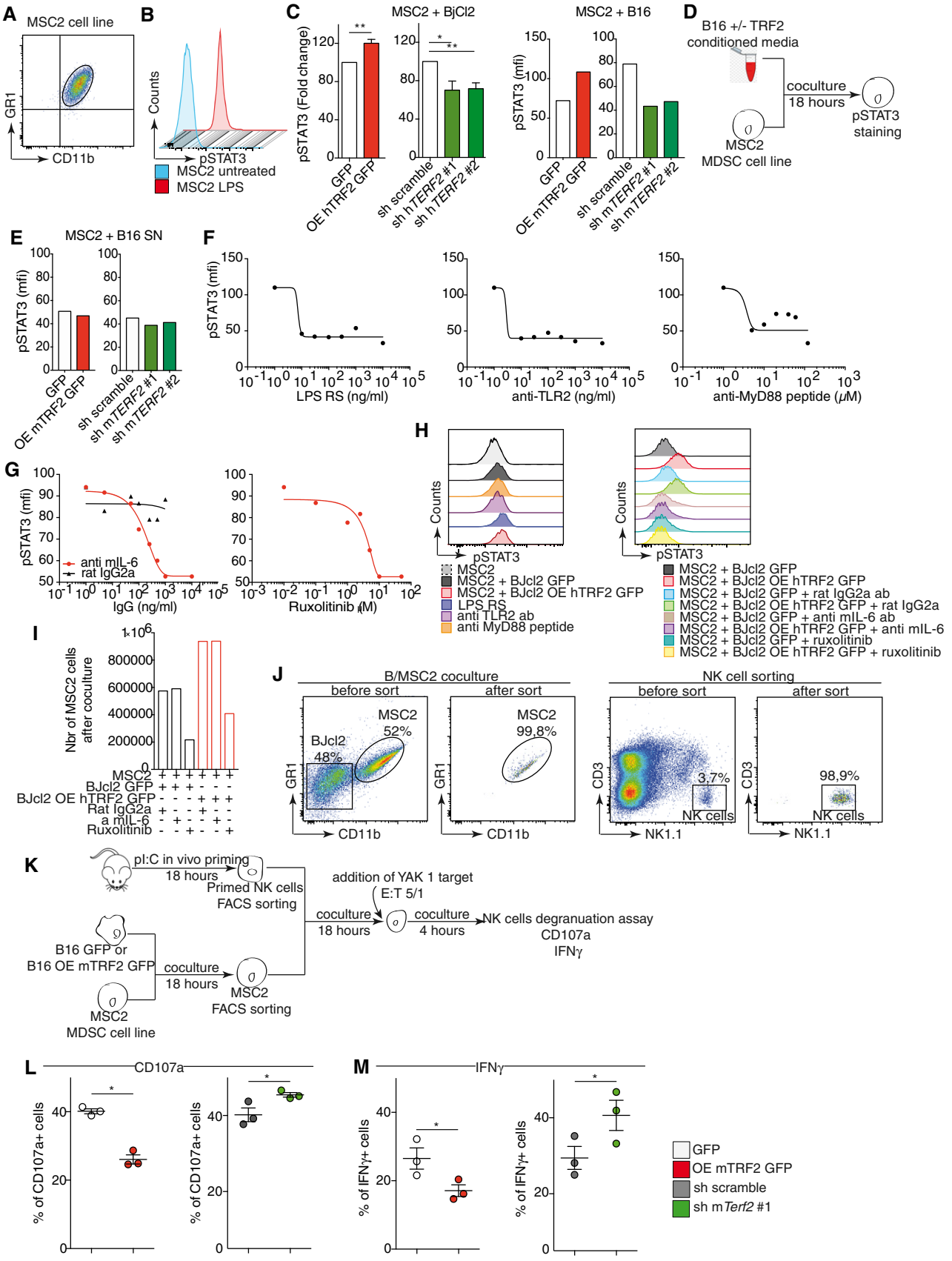

Figure EV3.

Figure EV4. TRF2 regulates the expression of a set of ITS-associated genes involved in HSPG biosynthesis.

A qPCR analysis of TRF2 expression in BJcl2 cells in which TRF2 target gene expression was determined in Fig 4A and D.
B FACS analysis of GPC6 and VCAN expression in BJcl2 cells overexpressing or compromised for TRF2
C Western blot analysis of HS3ST4, GPC6, and VCAN expression in BJcl2 cells overexpressing or compromised for TRF2
D Analysis of the correlation among the genome size (*y*-axis), total number of ITSs (*z*-axis corresponding to sphere diameter), and number of ITSs containing H3K27ac peaks (*x*-axis).
E–G Correlation between genome size and total number of ITSs (D), between total number of ITSs and number of ITSs containing H3K27ac peaks (F), and between total number of ITSs and number of ITSs containing H3K4me3 peaks (G)
H Venn diagram of genes identified by TRF2 chromatin immunoprecipitation sequencing (ChIP-seq; red), genes bearing ITSs (blue), and all H3K27ac peaks (green).
I Histograms of the percentage input of total H3 or input of H3K27ac used for immunoprecipitation or the ratio of the percentage input of total H3 to that of H3K27ac used for immunoprecipitation for the HS3ST4 ITS.

Data information: In (D–G), Pearson correlation and *P*-values are indicated.

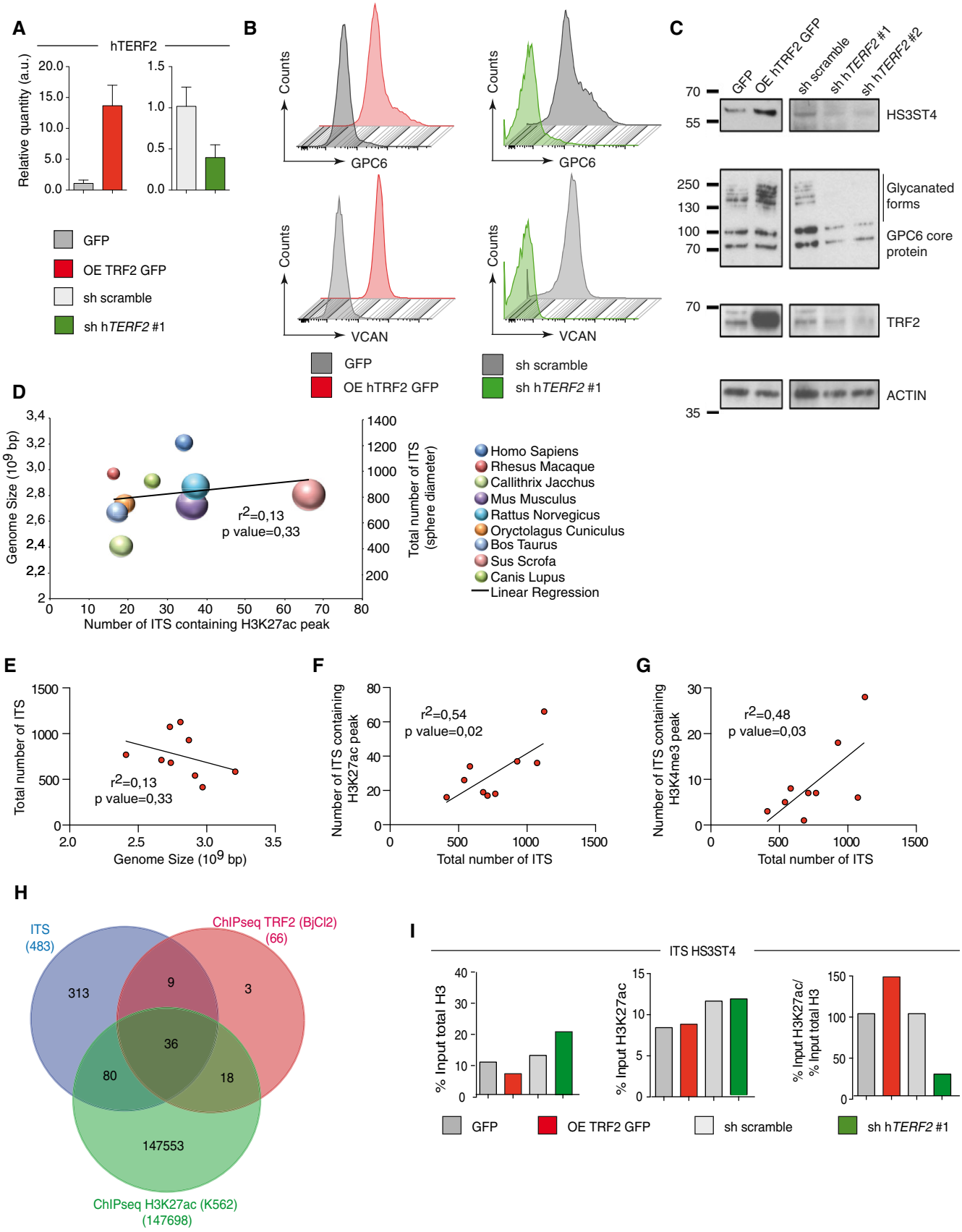

Figure EV4.

Figure EV5. TRF2 upregulation enhances glycocalyx stiffness, which activates MDSCs, enhances the response to chemotherapies targeting MDSC, and decreases overall survival (related to Figs 6–8).

A Graphical model arising from our main results.

B–E Kaplan–Meier curves for overall survival of chemotherapy- or surgery-treated patients with breast (B), gastric (C), ovarian (D), or lung (E) cancer according to the TRF2 expression level (KM-plotter, http://kmplot.com/analysis/index.php?p=background).

F RNAseq analysis of *TERF2* expression of 30 types of malignancies compared with normal tissues. Cases harboring mutations are depicted in the graph.

G The numbers, frequencies, and locations of mutations in the *TERF2* gene among 13,490 sequenced cases.

H–J The overall survival of gastric cancer patients (all stages) was analyzed depending on the expression level of HS3ST4 (H) or GPC6 (I) or VCAN (J) compared to TRF2 expression using KM-plotter.

K Table summarizing the median of survival (months), *P*-values, and hazard ratio depending on TRF2, HS3ST4, GPC6, or VCAN expression.

L Venn diagram associated with Fig 7F showing the intersection between the three categories of patients.

Data information: The optimal cut-off is determined on KMplot. The *P*-value (log-rank test), the hazard ratio, and number of patients are indicated in Dataset EV6.

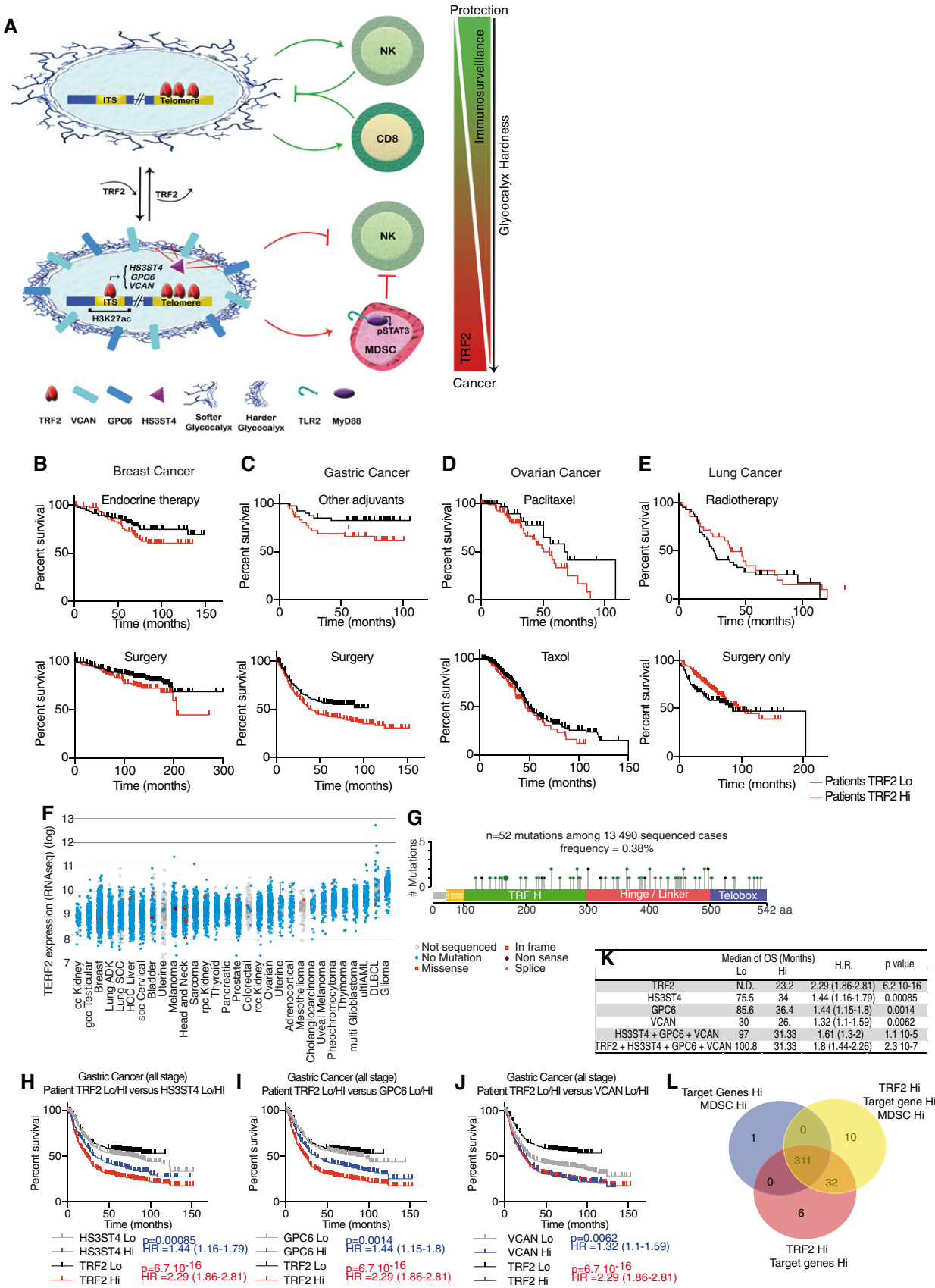

Figure EV5.